# Collective ion dynamics in ionic plastic crystals: The origin of conductivity suppression

Ivan Popov<sup>1\*</sup>, Haijin Zhu<sup>2</sup>, Airat Khamzin<sup>3</sup>, Curt Zanelotti<sup>4</sup>, Louis Madsen<sup>4</sup>, Maria Forsyth<sup>2,5</sup>, Alexei P. Sokolov<sup>1,6§</sup>

## **Abstract**

Organic ionic plastic crystals (OIPCs) appear as promising materials to replace traditional liquid electrolytes, especially for use in solid state batteries. However, OIPCs show low conductive properties relative to liquid electrolytes, which presents an obstacle for their widespread applications. Recent studies revealed very high ion mobility in solid phases of OIPCs, yet the ionic conductivity is significantly (~100 times) suppressed because of strong ion-ion correlations. To understand the origin of the ion-ion correlations in OIPCs, we employed broadband dielectric spectroscopy, light scattering and NMR diffusion measurements in liquid and solid phases of Hexafluorophosphate - Diethyl(methyl)(isobutyl)phosphonium [PF6][P1,2,2,4]. The results confirmed significant decrease in conductivity of solid phases of this OIPC through ion-ion correlations. Surprisingly, these ionic correlations suppress charge displacement on rather long time scales comparable to the time of ion diffusion on the ~1.5 nm length scale. We ascribe the observed phenomena to momentum conservation in motion of mobile anions and emphasize that microscopic understanding of these correlations might enable design of OIPCs with strongly enhanced ionic conductivity.

## Introduction

Solid state batteries (SSBs) are considered to provide a next breakthrough in mobile electrical energy storage technology [1-3]. However, development and implementation of SSBs is strongly hindered by properties of solid electrolytes. Organic ionic plastic crystals (OIPCs) are one class of promising materials to replace liquid electrolytes in energy storage and other electrochemical

<sup>&</sup>lt;sup>1</sup>Department of Chemistry, University of Tennessee, Knoxville, Tennessee 37996, USA

<sup>&</sup>lt;sup>2</sup>Institute for Frontier Materials, Deakin University, Burwood, Victoria 3125, Australia

<sup>&</sup>lt;sup>3</sup>Institute of Physics, Kazan Federal University, Kazan, Tatarstan 420008, Russia

<sup>&</sup>lt;sup>4</sup>Department of Chemistry and Macromolecules Innovation Institute, Virginia Tech, Blacksburg, Virginia, 24061, USA

<sup>&</sup>lt;sup>5</sup>ARC Centre of Excellence for Electromaterials Science (ACES), Deakin University, Burwood, Victoria 3125, Australia

<sup>&</sup>lt;sup>6</sup>Chemical Sciences Division, Oak Ridge National Laboratory, Oak Ridge, Tennessee 37831, USA

devices [4-7]. Their nonflammability, absence of liquid phase, and negligible vapor pressure makes OIPCs very attractive for the next generation of safe batteries. Many OIPCs demonstrate relatively high conductivity, especially when doped with Li or Na salts [8-10]. Several studies indeed demonstrate that the doped OIPCs work in a battery, providing a potential solution for SSBs [11, 12].

However, unlike superionic ceramics, OIPCs have insufficient conductivity at ambient conditions due to strong conductivity suppression in their solid phases [4, 7, 13-20]. Earlier studies revealed that ion conductivity usually shows step-like decreases in conductivity between different phases, while diffusion coefficient of mobile ion shows surprisingly smooth temperature variations [7, 16]. In recent analysis [7] this interesting behavior of two ion transport characteristics was related to correlations in ions dynamics. In simple terms, conductivity depends on velocity correlations of all ions, while diffusion reflects only the contribution from self-correlations. Indeed, by the definitions we have [21-23]

$$\sigma_{DC} = \frac{q^2}{3Vk_BT} \int_0^\infty \langle \sum_{i,j} \vec{v}_i(0) \cdot \vec{v}_j(t) \rangle dt \qquad D_i = \frac{1}{3} \int_0^\infty \langle \vec{v}_i(0) \cdot \vec{v}_i(t) \rangle dt \qquad (1)$$

where  $q_i$  and  $\vec{v}_i$  are charge and velocity of *i*-th ion, V is volume. Thus, self-correlations, which are always positive and define diffusion, are only part of the total conductivity. In turn, the distinct ion-ion correlations might have a negative sign and might reduce the total conductivity, although they might also be positive and enhance conductivity, the effect known for superionic ceramics [24-30]. Thus, controlling ionic correlations might significantly improve conductivity of electrolytes. In regular ionic liquids, the conductivity reduction (traditionally called "ionicity") usually is not large, (about 2-3 times) [31-38]. However, in many potential candidates for electrolytes in SSB, such as poly-ionic liquids and OIPCs, ion-ion correlations suppress ionic conductivity more than 100 times [13-15, 18-20, 39-47]. This strong effect requires comprehensive studies for the future development of novel electrolytes.

This manuscript provides detailed analysis of conductivity spectra and ionic correlations in OIPC  $[PF_6][P_{1,2,2,4}]$ : Hexafluorophosphate  $(PF_6)$  – Diethyl(methyl)(isobutyl)phosphonium  $(P_{1,2,2,4})$ . The conductivity measurements cover the extremely broad frequency range from 0.1 Hz to ~30 GHz, and are complimented by light scattering and NMR measurements. The analysis revealed unusual two-step conductivity spectra in OIPCs with the first step related to the usual local ion

rearrangement step observed also in the ionic liquid state, with the second step developing at lower frequencies. We demonstrate that the second step is controlled by strong correlations in dynamics of mobile ions which appears to be time dependent. We propose a method of analysis of time dependence of ionic correlations based on conductivity spectra and nuclear magnetic resonance (NMR) diffusion data. Moreover, our analysis suggests that these correlations are developing on a length scale comparable to the size of crystalline unit cell in OIPC. Based on these results, we propose ways to control these correlations and enhance conductivity in OIPCs.

## Material and experimental measurements details.

<u>Material</u>. Hexafluorophosphate (PF<sub>6</sub>) – Diethyl(methyl)(isobutyl)phosphonium (P<sub>1,2,2,4</sub>) was prepared as described in [16] (see Scheme 1). The structural characterization of this material is given in [16], where it was shown that [PF<sub>6</sub>][P<sub>1,2,2,4</sub>] has melting temperature  $T_m\sim 423K$ , and several solid-solid phase transitions (resulting in plastic crystal phases) at lower temperatures.

**Scheme 1**. Chemical structure of [PF<sub>6</sub>][P<sub>1,2,2,4</sub>]: Hexafluorophosphate Diethyl(methyl)(isobutyl)phosphonium.

Conductivity spectra measurements were performed using three setups to cover the wide frequency range from 0.1 Hz up to 50 GHz. The sample was dried in a vacuum oven at 323K for two days before measurements. An Alpha-A analyzer from Novocontrol was utilized in the frequency range of 10<sup>-1</sup> Hz to 10<sup>6</sup> Hz. A cell consists of a cap as a bottom electrode; the upper electrode is separated from the cap by a sapphire window to avoid electrical contact between them. The fixed electrode distance of 0.4 mm and diameter of 10.2 mm were used. The samples were measured with a voltage amplitude of 0.1 V. The standard calibration procedure was used before measurements. An Agilent RF Impedance Material Analyzer, E4991A with WinDETA Software from Novocontrol were used in the frequency range 10<sup>6</sup> Hz to 3·10<sup>9</sup> Hz. The cell was constructed from two APC-7 connectors. For the upper electrode, the inner pin of one connector was replaced

by a solid pin with diameter 3mm and the free space between inner pin and outer part was filled by Teflon. For lower electrode, the pin in another connector was removed and in the free central space a movable metallic cylinder was inserted. As a result, the coaxial line was terminated by the plate capacitor with adjustable distance between the electrodes. The coaxial line was calibrated using standard procedure (Open/Short/50 Ohm) to move the reference plane up to cell terminating the line. The cell was calibrated as well (Open and Short) for better precision. The samples were loaded between two electrodes with distance 0.1mm and measured with a voltage amplitude of 0.1V. The Panoramic Network Analyzer, Agilent Technologies, E8364C with 85070E Dielectric Probe Kit were utilized for frequency measurements from 5·10<sup>8</sup> Hz up to 5·10<sup>10</sup> Hz. The Performance Probe with the Agilent Electronic Calibration module (ECal) were used for measurements of real and imaginary part of dielectric permittivity. The calibration was performed in standard procedure using Open, Short (Performance Probe Kit) and Load (Distilled water at 20°C) states. Just before each measurement the calibration was refreshed using ECal module. A Quattro temperature controller (Novocontrol) was used for temperature stabilization for the measurements from 10<sup>-1</sup> Hz to 10<sup>9</sup> Hz. The samples were stabilized for 20 minutes at each temperature to reach precision ±0.2 K. The Presto, Julabo, W80 temperature controller sensor and heat plate was used for the measurements from 5·10<sup>8</sup> Hz up to 5·10<sup>10</sup> Hz. The samples were stabilized for 40 minutes at each temperature. A glovebox was used to load the samples in a hermetic dielectric cell.

Pulsed-gradient stimulated-echo (PGSTE) NMR was applied for diffusion measurements in the temperature range from 343K to 413K. Self-diffusion coefficients of ions were obtained by measuring the nuclei <sup>1</sup>H (cation diffusion) and <sup>19</sup>F (anion diffusion). Diffusion measurements from 343K to 413K were performed using a 600 MHz Bruker Avance III NMR spectrometer equipped with DOTY 5 mm, Standard VT, 1H/X high gradient pulsed-field-gradient (PFG) probe. The sample was prepared to match the protocol used for conductivity measurements with the following changes. The sample was dried in a vacuum oven for three days at 373K then loaded into an NMR tube and transferred to a vacuum line for further drying at 373K while under vacuum. Once dried the sample was flame sealed, to prevent any residual water uptake, and melted at just above 423K. The melted sample was then transferred to a refrigerator at 276K for 1 day. Additional experimental details are provided in SI.

Light Scattering (LS) was measured using Raman spectrometer and tandem Fabry-Perot (TFP) interferometer. The experiments were performed in backscattering geometry using laser wavelength 532 nm. To obtain wide frequency range, three mirror spacing were used in TFP interferometer: 0.4mm, 3mm, and 15 mm. Optical response from the same spot in the sample was transferred by additional mirrors to the T64000 Raman spectrometer from Horiba Jobin Yvon. Raman spectra were measured with CCD-camera in subtractive mode. High frequency Raman modes were used to normalize spectra at different temperatures. A glovebox was used to load the samples in a glass vial and seal. The sample was melted in cryostat, stabilized for 1 hour and measured at 433K. After this, it was cooled down to 410K, where the sample crystalized forming Phase I. After temperature stabilization for one hour, the light scattering spectra were measured. To remove the contribution of longitudinal modes from the light scattering spectra, the sample was measured in HV and HH polarizations at the same mirror spacing.

## **Experimental Results**

Traditionally, conductivity spectra exhibit 3 regimes [48] (Figs. 1): (i) Electrode polarization (EP) effect at low frequencies presenting a decrease of conductivity due to the accumulation of charge carriers at the surface of electrodes; (ii) Followed by a plateau level of DC conductivity regime at the intermediate frequencies; and (iii) AC regime at higher frequency. However, in solid state the studied OIPC demonstrates additional relaxation process (we note this as Process I) that appears as an additional step in conductivity spectra at frequencies slightly lower than that of the AC-DC crossover (Fig. 1). This process shows up as a clear peak in the imaginary part of the dielectric permittivity, and exists in all solid phases (see Fig. 1b,c). In contrast, the conductivity spectra of the melt shows traditional AC-DC crossover with no signature of this process (Fig. 1c), indicating that the Process I is related to specific dynamics in the crystalline structure of the OIPC.

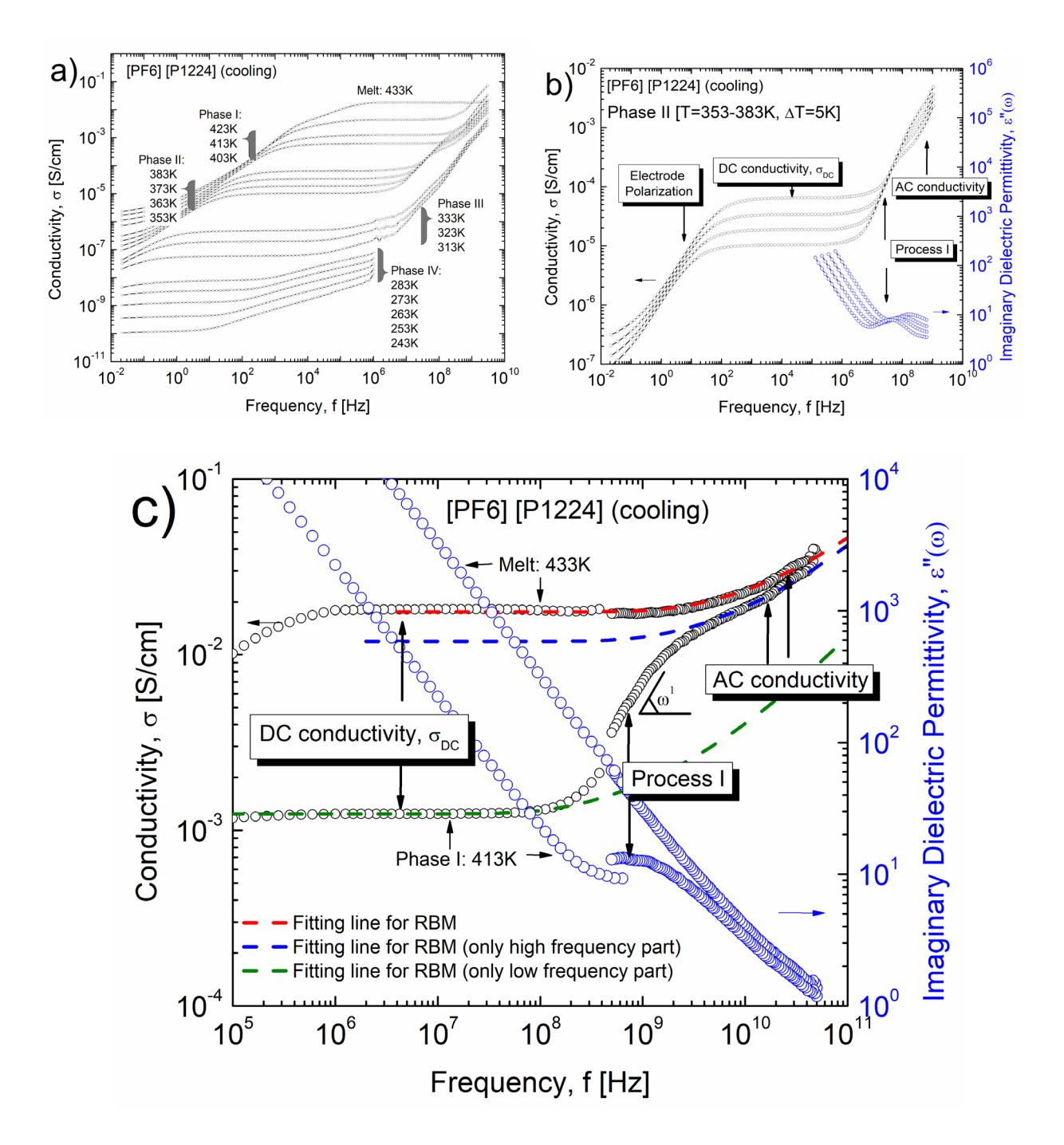


**Figure 1. a)** Conductivity spectra of [PF<sub>6</sub>][P<sub>1,2,2,4</sub>] in different solid phases and in melt state. **b)** Conductivity spectra and imaginary dielectric permittivity of [PF<sub>6</sub>][P<sub>1,2,2,4</sub>] in Phase II. **c)** Conductivity spectra and imaginary dielectric permittivity of [PF<sub>6</sub>][P<sub>1,2,2,4</sub>] in Phase I and melt state measure up to 50 GHz. The dashed lines are the fit to RBM model, Eq.(4).

Taking the plateau between electrode polarization and Process I, we obtain the temperature dependence of DC conductivity,  $\sigma_{DC}(T)$ , (Figure 2a). We also presented temperature dependence

of  $\sigma_{DC}(T)$  from our previous studies [7, 16]. DC conductivity shows clear steps at temperatures of the phase transitions, and hysteresis between cooling/heating cycles, especially in low temperature solid phases. In high temperature solid phases (Phase II and I) and in the melt the hysteresis is negligible. At the same time, the ion diffusivity measured by NMR for fast fraction of both ions doesn't show any steps between phases (see Figure 2b) and follows well a Vogel-Fulcher-Tammann (VFT) behavior. However, the steps between phases are observed in the populations of the fast diffusing ions, especially for the cation [16]. Additional discussion of NMR spectroscopy and diffusion results regarding mobile ion populations is provided in SI.

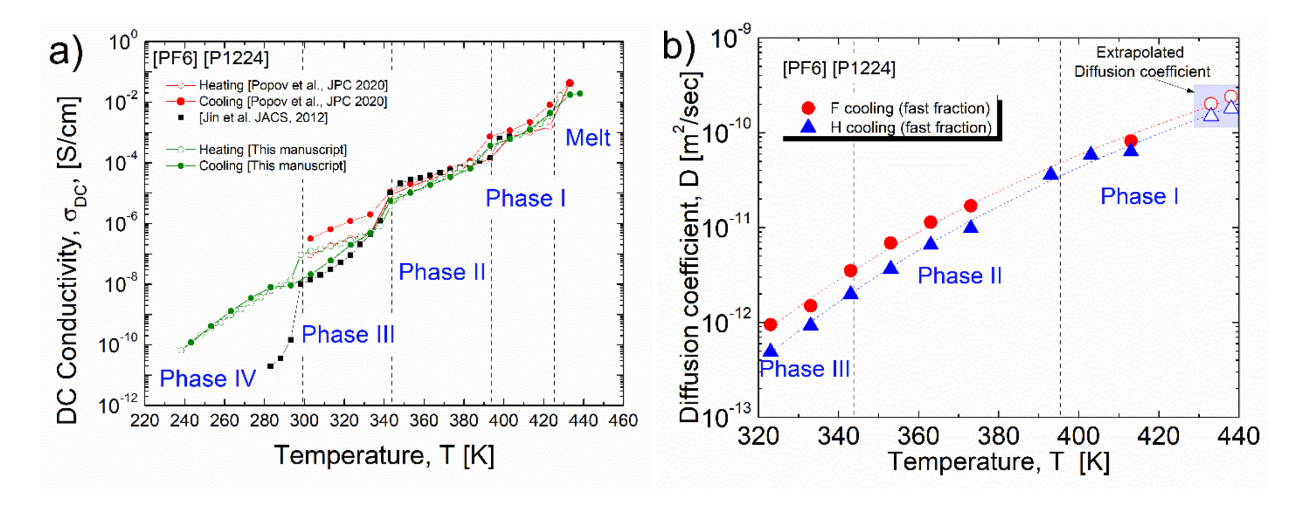


**Figure 2. a)** Temperature dependence of DC-conductivity of [PF<sub>6</sub>][P<sub>1,2,2,4</sub>] in solid and melted states. **b)** Diffusion coefficient of ions in [PF<sub>6</sub>][P<sub>1,2,2,4</sub>]. Solid symbols present data taken from [7] and newly measured data at 413K. Open symbols are extrapolated values of diffusion coefficient at higher temperature in melted state using VFT law.

The light scattering susceptibility spectra (analogous to the dielectric loss spectra) exhibit very broad structural relaxation peak around ~8 GHz in the melt state (T=433K), which corresponds to characteristic relaxation time ~0.02 ns. The peak has only a slight shift to lower frequency in the Phase I (Fig. 3). Thus, the light scattering reveals similar structural dynamics in the melt and in the Phase I. Comparison to the conductivity spectra (Fig. 3) reveals that the structural relaxation process measured in light scattering coincides with the AC-DC crossover in the melt. In solid state, in Phase I, the light scattering relaxation process also coincides with the initial AC-DC crossover. At the same time, the dielectric Process I at lower frequencies in Phase I is not observed in the light scattering spectra.

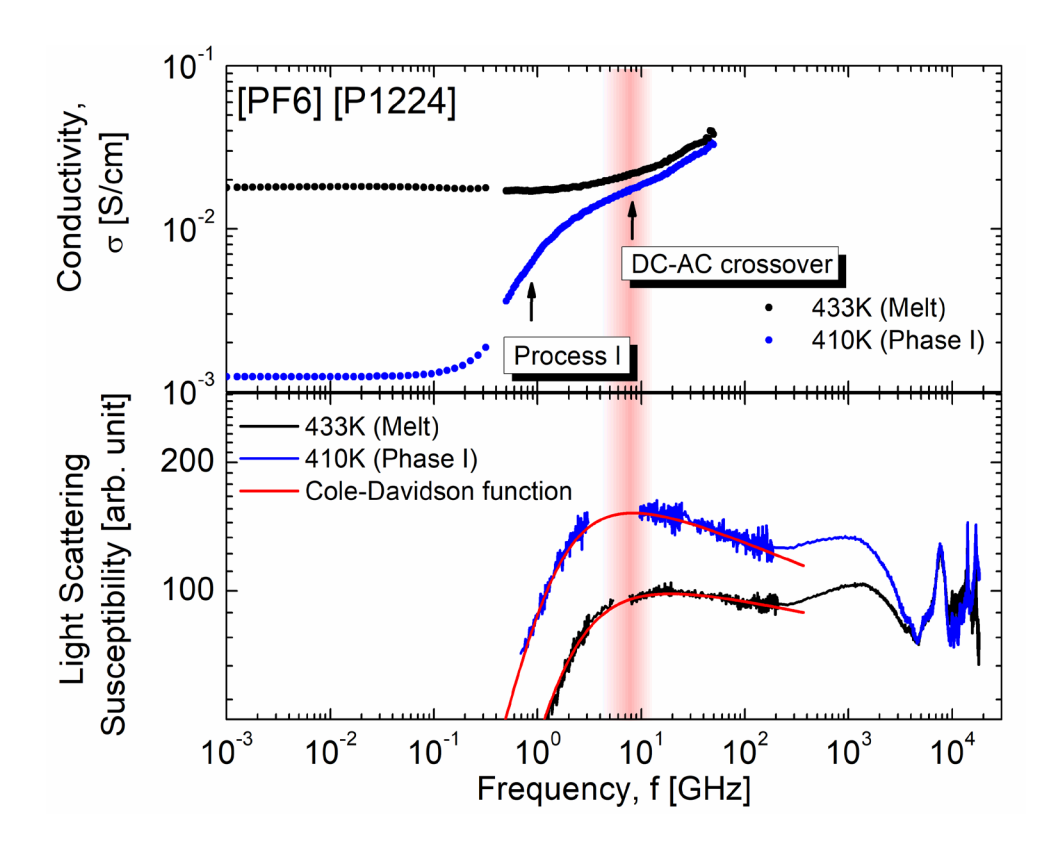


**Figure 3**. Comparative figure of conductivity (upper panel) and light scattering (lower panel) spectra of [PF<sub>6</sub>][P<sub>1,2,2,4</sub>] in solid Phase I and melted states. Red lines in light scattering susceptibility spectra are fit to Cole-Davidson function. The positions of maximum in relaxation peak of light scattering susceptibility and DC-AC crossover in conductivity spectra are highlighted by red rectangle.

## **Discussion**

The most surprising and intriguing result of our experimental studies is that diffusion coefficient of the fast ions shows smooth temperature variations between different solid phases (Fig. 2b), and structural relaxation time measured by light scattering does not change significantly between melt and solid state (Fig. 1c), while conductivity decreases step-like between different phases (Fig. 1c, 2a). Moreover, the conductivity spectrum in the melt shows classical behavior, while an additional step in conductivity spectra appears in solid phases (Fig. 1). To understand these effects, we need to go back to fundamentals of ion diffusion and conductivity. By definition (Eq. 1), diffusion is a measure of velocity-velocity self-correlation function, while conductivity measures velocity-velocity correlations for all the ions (including cross-correlations), and distinct ion-ion correlations

can significantly suppress or enhance conductivity [30, 49, 50]. Thus, the drop in conductivity between solid phases without a drop in ion diffusion, might be related to step-like changes in ionion correlations. Classical expression for ionic conductivity, the Nernst-Einstein (NE) equation assumes independent ionic contributions and neglects ion-ion correlations [21-23, 35]:

$$\sigma_{NE} = \frac{nq^2}{k_B T} (\phi_+ D_+ + \phi_- D_-)$$
 (2)

Here  $k_B$  is the Boltzmann constant,  $\phi_{\pm}$  and  $D_{\pm}$  are mobile fraction and diffusion coefficient of cation (+) and anion (-). Here we assume that both anion and cation have the same charge q, and concentration n, but have a difference in translationally mobile fraction of anion  $\phi_{-}$  and cations  $\phi_{+}$ . However, ion dynamics in concentrated ionic systems are strongly correlated [7, 49], and this leads to significant deviation of experimentally measured conductivity  $\sigma_{DC}$  from the prediction of NE equation based on knowledge of the ion diffusion. This deviation is usually characterized by the 'ionicity' or inverse Haven ratio [51-58]. The latter can be defined as:

$$H^{-1} = \frac{\sigma_{DC}}{\sigma_{NE}}. (3)$$

Having diffusion, fraction of fast ions and conductivity data we can estimate the effect of ion-ion correlations in different phases calculating the inverse Haven Ratio,  $H^1$ . From the earlier studies [7, 16, 59] we have an estimation of the fast mobile ion fractions and know that in phase III and II only anions (PF<sub>6</sub>) are mobile, while in phase I, both ions are mobile. Unfortunately, we couldn't measure ion diffusion in the melt due to the temperature limitations of the PFG-NMR equipment used. However, no significant changes in characteristic structural relaxation time between melt and Phase I (DLS data, Fig. 3b) suggests that the diffusion of ions also will not change significantly. Furthermore, the AC-DC crossover (which is related to ion diffusion) in the melt and initial AC-DC crossover in the Phase I also happens at approximately the same frequencies (Fig. 1c), additionally supporting the assumption that ion diffusion does not change significantly. Based on this assumption, we extrapolated the VFT behavior of diffusion coefficient observed in the solid state to estimate the diffusion of ions in the melt at T=433K (Fig. 2). Of course, both ions are expected to be mobile in the melt.

Based on this, we can obtain the temperature dependence of the inverse Haven ratio using Eq. (3). Analysis reveals (Fig. 4) that the inverse Haven ratio in the melt has a value comparable to other

ionic liquids  $H^{-1} \sim 0.5$ -0.7 [31-38]. However, in the solid states it drops significantly and decreases to less than 0.01 in Phase III. These results demonstrate the significant role of ion-ion correlations in solid phases of this plastic crystal.

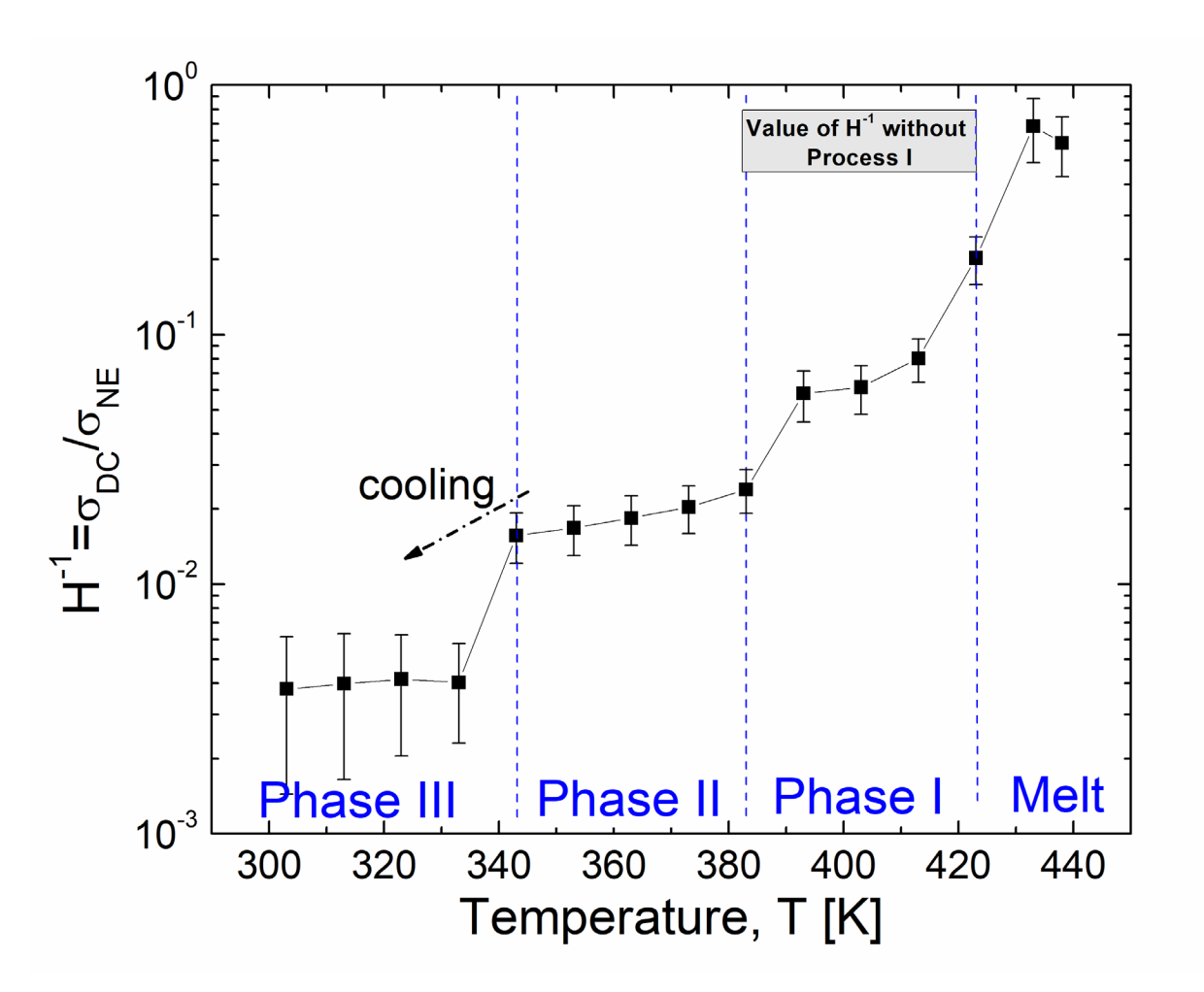


**Figure 4**. Temperature dependence of the inverse Haven ratio of [PF<sub>6</sub>][P<sub>1,2,2,4</sub>] in solid and melted states. In the melt state the inverse Haven ratio is  $\sim$ 0.5, which is comparable to other ionic liquids, however it significantly drops in solid phases. The estimation of inverse Haven ratio without Process I in Phase I is shown by grey rectangle. For this estimation we used DC conductivity which provided by Eq.(4) (blue line in Fig.1c)

Thus, our analysis clearly suggests that the drops in conductivity between different phases of the studied OIPC is caused mostly by the drops in the inverse Haven ratio. The conductivity spectra in all solid phases clearly show (Fig. 1) that after initial AC-DC crossover there is an additional drop to reach the final DC regime, and the associated Process I in the dielectric permittivity. The

typical AC-DC crossover in conductivity spectra of ionic liquids corresponds to a crossover of ion motion from a rattling in a coulombic cage created by neighbor ions (corresponding to AC tail and sub-diffusive regime) to normal long range diffusion, when ions re-arrange and escape from this cage (corresponding to DC-plateau) [60-64]. It has been demonstrated for many ionic liquids that this crossover happens at the structural relaxation time measured, e.g., by light scattering or rheology [65, 66]. Indeed, we observe this type of behavior for the melt (Fig. 1c) indicating that the studied ionic system in its melt state behaves as a usual ionic liquid. However, in solid phases the initial ion rearrangement, although providing an initial AC-DC crossover, does not result in DC conductivity, and an additional mechanism suppresses DC conductivity at longer time (lower frequencies).

It is well-known that the AC-DC crossover in conductivity spectra is well described by Random Barrier Model (RBM) [60-64]. This model suggests that the transport of charge carriers happens by hops over some percolation potential energy barriers. In the case with a constant barrier height distribution the model leads to the equation [60, 64]

$$\ln\left(\frac{\sigma^*(\omega)}{\sigma_{DC}}\right) = \frac{i\omega\tau_{\sigma}\sigma_{DC}}{\sigma^*(\omega)} \left(1 + \frac{8}{3} \frac{i\omega\tau_{\sigma}\sigma_{DC}}{\sigma^*(\omega)}\right)^{-1/3}.$$
 (4)

Here  $\sigma^*(\omega)$  is a complex conductivity;  $\sigma_{DC}$  is a DC-conductivity, and  $\tau_{\sigma}$  is a conductivity relaxation time. The latter defines the characteristic AC-DC crossover time, i.e., when charge sub-diffusive regime crosses over to a normal diffusion regime  $\langle r^2(t) \rangle \sim t$  (here  $\langle r^2(t) \rangle$  is the charge mean-squared displacement). Eq. (4) provides a good fit to the conductivity spectra in the melt (Fig. 1c). The same Eq. (4) provides a good fit to the initial AC-DC crossover in Phase I (Fig 1c), and also enables estimates of the possible DC conductivity and inverse Haven ratio without the second drop. This analysis reveals the initial value of H<sup>-1</sup>~ 0.5-0.7 expected in Phase I (Fig. 4), is close to the values for the melt state. Furthermore, taking the value of  $\tau_{\sigma}$  from the fit of the conductivity spectra to the Eq. (4) (Fig. 1c), we can estimate the rearrangement length, when ions escape coulombic cage and should reach normal diffusion regime, using the relationship [35, 36, 42, 65]

$$\lambda_{AC-DC} = \sqrt{6D\tau_{\sigma}} \tag{5}$$

Here D is a diffusion coefficient of ions measured from PFG-NMR. The value of  $\lambda_{AC-DC}$  in Phase I and melt states appears to be  $\sim 1-2$  Å (Fig 5b). This value for rearrangement length is typical for

ionic liquids and is comparable to half a distance between the mobile ions. The similar value of rearrangement length in solid and melted state of plastic crystal indicates that, at least at short time and short length scales, the ion dynamics and rearrangements even in solid state behave like in the ionic liquid. The significant changes in ion transport occur at longer time (or lower frequencies) when an additional mechanism suppresses ionic conductivity.

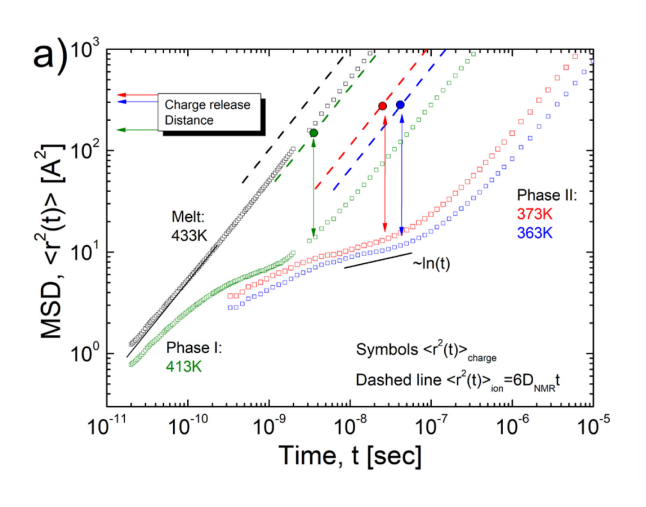
We note that the slope of Process I in conductivity spectra is close to  $\sim \omega^1$ , which is much steeper than predicted for the AC-regime by the RBM (see the green dashed line in Fig.1c). Using the relationship between conductivity spectra and the mean square displacement (MSD) of charge  $\langle r^2(t)\rangle_{charge}$  [23]

$$\sigma^*(\omega) = -\omega^2 \frac{nq^2}{6k_B T} \int_0^\infty \langle r^2(t) \rangle_{charge} e^{-i\omega t} dt$$
 (6)

we find that this behavior corresponds to the case when MSD is a slow time dependent function  $\langle r^2(t)\rangle_{charge} \propto \ln(t)$  (leading to  $\sigma(\omega)\sim\omega^1$ ). We emphasize that here  $\langle r^2(t)\rangle_{charge}$  is a mean square dependence of charges, not ions, and it includes also ion cross-correlations. Moreover, we can make a further step and use conductivity spectra and the inverse transform of Eq.(6) [23] to calculate the charge MSD, which accounts for all ion correlations  $\langle r^2(t)\rangle_{charge}$ .

$$\langle r^2(t)\rangle_{charge} = \frac{24k_BT}{nq^2\pi} \int_0^\infty \frac{\text{Re}[\sigma^*(\omega)]}{\omega^2} \sin^2\left(\frac{\omega t}{2}\right) d\omega \tag{7}$$

These time dependences in melt and solid phases are presented in Fig 5a together with MSD of fast ions estimated from NMR diffusion coefficient:  $\langle r^2(t) \rangle_{ion} = 6D_{NMR}t$ .



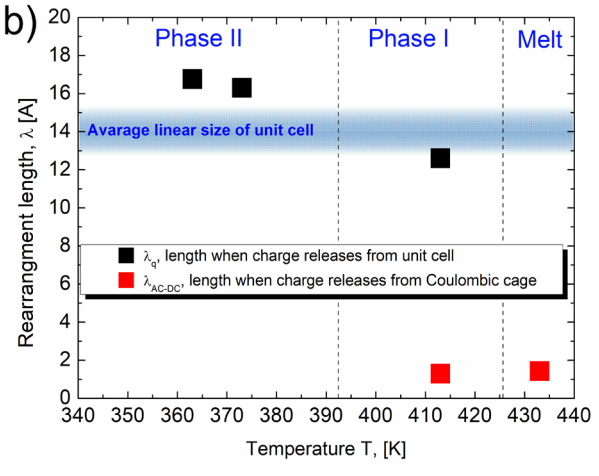


Figure 5. a) MSD of charge (symbols) estimated from the conductivity spectra using Eq.(7), and MSD of ions (lines) estimated using PFG-NMR in millisecond time scale and interpolated to shorter times,  $\langle r^2(t) \rangle_{ion} = 6 D_{NMR} t$ . b) Rearrangement length when charge releases from Coulombic cage,  $\lambda_{AC-DC}$ , estimated from AC-DC crossover and rearrangement length when charge is released from elementary unit cell,  $\lambda_q$ , estimated from Fig 5a. To estimate  $\lambda_q$  we took value of  $\lambda_q = \sqrt{\langle r^2(t) \rangle_{ion}}$  at times where  $\langle r^2(t) \rangle_{charge}$  reaches normal diffusion regime after being captured, when  $\langle r^2(t) \rangle_{charge} \propto \ln(t)$ . The shadow area shows the average linear size of elementary unit cell taken from [16].

This analysis revealed that in the melt state the charge reaches the normal diffusion regime very fast and its MSD is only ~ 2 times smaller than ion MSD (Fig. 5a), reflecting the value of H<sup>-1</sup>. In solid phases the initial sub-diffusive regime of charge has an MSD also close to that expected from the NMR ion MSD (dashed line), reflecting similarity of local dynamics (on scale ~1-2 Å) in solid and liquid phases. However, the charge MSD starts to increase very slow at longer times (as ln (t)), and reaches a normal diffusion regime with significant delay, resulting in charge MSD being much smaller than MSD of ions. Using again the relationship Eq.(5) and the characteristic time of crossover to DC conductivity, we can estimate the average distance of ion displacement at which the charge reaches the normal diffusion regime. The estimated time and distance are marked in Fig 5a. The value of  $\lambda_q \sim 1.5$ -2 nm appears significantly larger than the characteristic ion rearrangement scale,  $\lambda_{AC-DC}$  (Fig 5b). Surprisingly,  $\lambda_q$  is approximately equal to the average size of elementary unit cell of this plastic crystal ~1.3 -1.6 nm [16], suggesting that despite ion diffusion a charge remains confined on the scale of the crystalline elementary cell for a significant time. It remains a puzzle to understand how the size of crystalline cell might play a role in ionic correlations.

To analyze this unexpected results in more details, we suggest to rewrite the inverse Haven ratio in terms of MSD instead of diffusion coefficients:

$$H^{-1}(t) = \langle r^2(t) \rangle_{charge} / \langle r^2(t) \rangle_{ion}$$
 (8)

This enables the estimation of the time dependences of the inverse Haven ratio  $H^{-1}(t)$  from conductivity spectra (Fig 6). The so-obtained  $H^{-1}(t)$  is time independent in the melt, suggesting constant contribution of distinct ion-ion correlations in the accessible time range. However,  $H^{-1}(t)$  in the solid state is similar to the melt state at short time, but then drops significantly at longer time, reaching some saturation at much lower level at times when charge reaches normal diffusion

(Fig. 6). To the best of our knowledge, this is the first attempt to provide experimental analysis of the distinct ionic correlations as a function of time.

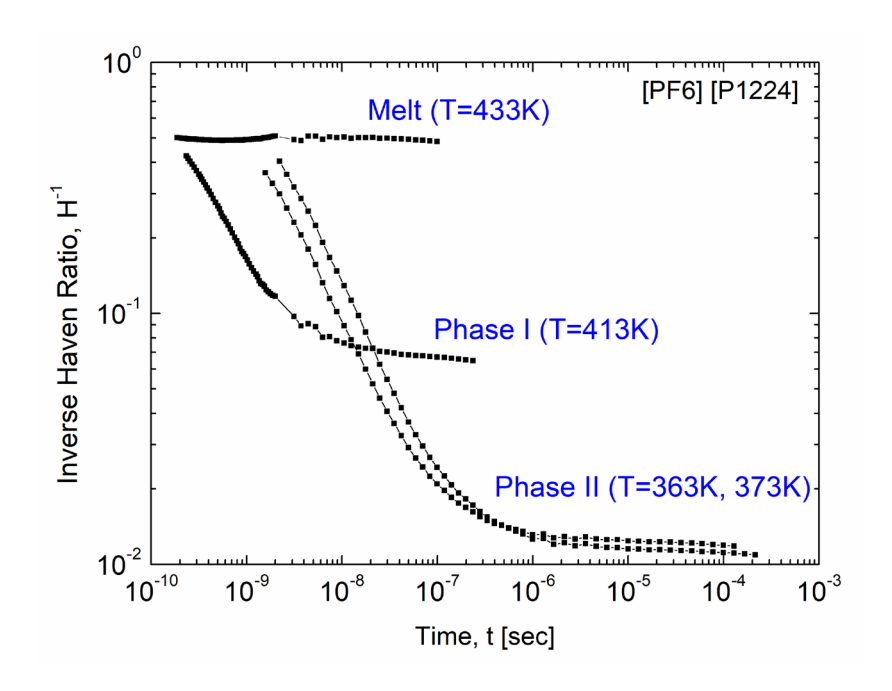


**Figure 6.** Time dependence of inverse Haven ratio obtained from Eq.(8) for [PF<sub>6</sub>][P<sub>1,2,2,4</sub>] in solid and melted states.

Summarizing all the experimental facts we propose the following scenario for the ion transport in the OIPC. In the liquid state, the ion transport behavior is essentially that of a regular ionic liquid, where ion correlations suppress conductivity  $\sim$  2-3 times. According to recent studies based on a momentum conservation approach [7, 49, 50, 67], the suppression mechanism in ionic liquids is mostly related to negative distinct cation-cation and anion-anion correlations, while distinct anion-cation correlations are positive and enhance conductivity. However, in solid states there are two types of ion dynamics (see scheme in Fig. 7). We may refer to the first type as an intra-cell dynamic. The X-ray diffraction shows [16] that in this OIPC the crystalline solid phase has an elementary unit cell with sizes  $\approx$ 1.3-1.6 nm, which contains eight [PF<sub>6</sub>][P<sub>1,2,2,4</sub>] ion pairs. On a local scale ( $\sim$ 1-2 Å), the ion dynamics are similar to regular ionic liquids, with similar ion-ion correlations. However, the ionic correlations suppress the charge displacement on a longer time and length scale, and a charge reaches the normal diffusion regime only when ions leave the unit cell. This type of ion transport we refer as an inter-cell dynamic. At the same time, the escape of

an ion from the crystalline cell breaks the cell charge neutrality. To restore it, another ion has to jump inside the unit cell. Thus, the charge fluctuation on the length of the unit cell, lead to fluctuation of the dipole moment,  $\mathbf{P}$ , which is proportional to  $\sim q*l$ , where q is an ion charge, and l is the size of the unit cell (see Fig.7). As a result, this fluctuation of the cell dipole moment,  $\mathbf{P}$ , leads to the appearance of the relaxation Process I.

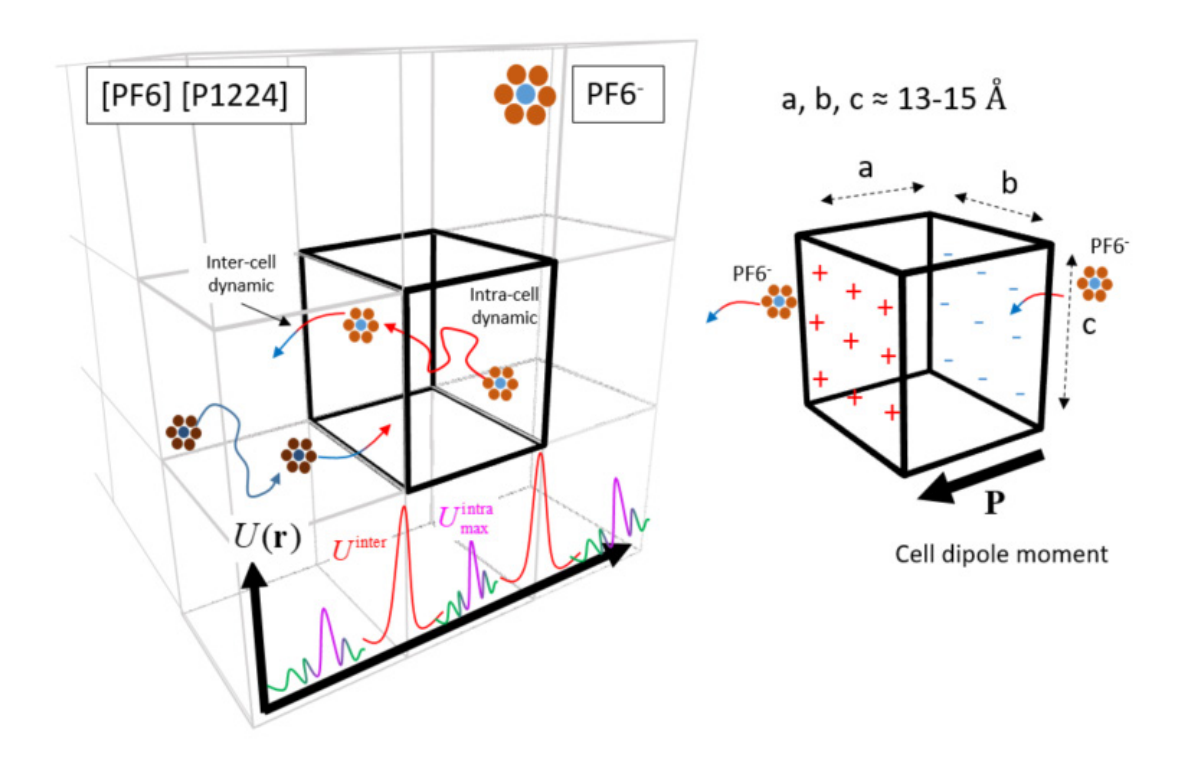


**Figure 7**. Schematic presentation of ion transport in [PF<sub>6</sub>][P<sub>1,2,2,4</sub>] in the solid phase. Two types of ion diffusion can be distinguished: i) intra-cell and ii) inter-cell. Intra-cell ion transport is similar to regular ionic liquid, while inter-cell dynamic requires ion transfer through the cell boundary. At inter-cell ion transport there is a strong backflow of PF<sub>6</sub>. This might happen either because of momentum conservation (between whole cell and PF<sub>6</sub> ion) or elementary cell charge neutrality. As a result, there is an ion diffusion, but charge diffusion is trapped at the scale of cell, leading to drop in conductivity and inverse Haven ratio. The same inter-cell ion transport provides charging of cell boundaries, leading to appearance of huge dipole moment, which we observe as a Process I.

This model explains why the relaxation time of the Process I (or its position in frequency range) coincides with the onset of the AC-DC crossover: Apparently the onset of normal charge diffusion regime is coupled with fluctuation of charge on the scale of the unit cell. Because the size of the unit cell, l, is larger than 10 Å, it provides a large value of cell dipole moment, and this explains

the high amplitude of the loss peak of the Process I in the dielectric spectra, and also explains why we see no signs of this process in the light scattering spectra. The light scattering shows responses only from intra-cell dynamics associated with local ions rearrangements. There are no crystalline cells in the melt, and thus no inter-cell dynamics. As a result, the Process I disappears in the melt. In contrast, local ion dynamic (i.e., intra-cell ion dynamic) exist in both melt and crystalline phases explaining why light scattering shows similar spectra in both phases (see Fig.3).

Although we currently don't have a clear microscopic explanation of the observed suppression of conductivity in OIPCs, we can suggest some qualitative general scenario. Some previous studies propose the role of vacancies in OIPCs [13, 14], however here we consider the analysis based on momentum conservation approach [7, 49, 50, 67], revealing that the major suppression of conductivity in solid phases of [PF<sub>6</sub>][P<sub>1,2,2,4</sub>] might be caused by negative anion-anion correlations, most probably due to a kind of backflow of PF<sub>6</sub>. The contribution of distinct ion-ion correlations based on momentum conservation law are described by the following equations [7, 49, 67, 68]

$$\sigma_{DC} = \sigma_{NE} + \sigma_{+-} + \sigma_{++}^d + \sigma_{--}^d$$
, where  $\sigma_{NE} = \sigma_{+}^s + \sigma_{-}^s$ , (9a)

$$\sigma_{++}^d = \sigma_{DC} \left( \frac{m_-}{m_- + m_+} \right)^2 - \sigma_+^s, \qquad \sigma_+^s = \frac{q^2 n}{k_B T} \phi_+ D_+,$$
 (9b)

$$\sigma_{--}^d = \sigma_{DC} \left( \frac{m_+}{m_+ + m_-} \right)^2 - \sigma_{-}^s, \qquad \sigma_{-}^s = \frac{q^2 n}{k_B T} \phi_- D_-,$$
 (9c)

$$\sigma_{+-} = 2\sigma_{DC} \frac{m_+ m_-}{(m_- + m_+)^2}.$$
 (9d)

Here  $m_+$  and  $m_-$  are the masses of cation and anions, respectively. Fraction of mobile ions  $\phi_\pm$  are taken from earlier studies [7, 16, 59]. From Eqs.(9) it is clearly seen that the distinct ion-ion correlations strongly depend on the mass ratio between cation and anion. At short time scale, the impact of anion-anion correlations for the intra-cell dynamic is small because the mass of cation and anion is comparable. However, at large timescale corresponding to the inter-cell dynamic, when anion leaves the cell, we can consider the whole elementary cell as a large effective cation instead of single  $P_{1,2,2,4}$  ion. In this case, when  $m_+ \gg m_-$ , Eqs.(9) lead to  $\sigma_{++}^d \to 0$ ,  $\sigma_{+-} \to 0$  and contribution of anion-anion correlations ( $\sigma_{--}^d$ ) becomes dominant. Because the conductivity is suppressed in solid phases unlike the diffusion, we have  $\sigma_{DC} \ll \sigma_-^s$  leading to anion-anion correlations with a negative sign. In other words, momentum conservation in the case of

immobilized cations requires the motion of one anion to be compensated by a motion of another anion in the opposite direction, suppressing charge displacement and DC conductivity (Fig. 5a). One way to reduce these negative correlations and eliminate anion backflow is the use of salt doping. According to recent studies [8-10], even a small amount of salt doping (few mole percent) often leads to huge increase in conductivity of OIPC's solid phases. We speculate that addition of small amount of salt leads to a distortion and decay of elementary unit cell in plastic crystal and as a result this leads to decreasing of ionic correlations on the length scale of elementary cell. This could also arise from a large increase in population of a mobile ions diffusing in a grain boundary or other dynamically separate phase. Both of these would lead to a significant increase in conductivity, and further investigations will be needed to test these hypotheses.

## Conclusion

The presented dielectric studies of [PF<sub>6</sub>][P<sub>1,2,2,4</sub>] system in a broad frequency and temperature range revealed unusual spectral shape of conductivity in solid phases. While liquid phase of this system shows usual AC-DC crossover, two characteristic regions appear in the conductivity spectra of solid phases. Moreover, the DC conductivity shows step-like changes between solid phases while fast anions diffusion shows smooth VFT-like temperature variations without steps across these phases. Also, the structural relaxation measured by light scattering shows similar behavior in the melt and solid phase. Characteristic frequency of the structural relaxation agrees well with the frequency of the AC-DC crossover in the melt, which is a usual behavior for ionic liquids. Our analysis demonstrates that the frequency of the faster crossover in conductivity spectra of the solid phase also agrees with the characteristic time of its structural relaxation. Based on this result, we ascribe the faster conductivity process to the local ion rearrangements in the solid phase, while the final AC-DC crossover at lower frequencies is ascribed to crossover of charge transport to a regular diffusion behavior. The obtained results suggests that local ion rearrangements are similar in the melt and solid phases and have rather smooth temperature variations, in agreement with the NMR ion diffusion measurements. This is in strong contrast with the step-like behavior of DC conductivity that reflects charge transport.

Direct comparison of NMR diffusion and conductivity data suggests that steps in DC conductivity between different phases is related to the step-like changes in ionic correlations. Essentially, reducing mobility of cations leads to strong increase in dynamic anion-anion correlations that

strongly suppress conductivity. Moreover, we demonstrate that using conductivity spectra and

NMR diffusion data one can analyze time dependence of these correlations presented as the inverse

Haven ratio. Analysis of this dependence reveals extended time range with no significant charge

displacement although anions are diffusing. We ascribe this suppression of charge transport by

momentum conservation in dynamics of anions. Only when ions diffuse on the length scale

comparable to the size of elementary crystalline cell of this OIPC do the ionic correlations reach a

steady-state regime and charge transport crosses over to the normal diffusion process. Presently

we don't have any clear microscopic explanation of this effect. We emphasize that detailed

understanding of the dynamic ionic correlations in OIPCs might enable design of plastic crystals

with strongly enhanced ionic conductivity.

**Supporting Information** 

NMR spectroscopy and diffusometry experimental details and additional results.

Acknowledgements

We acknowledge support by the National Science Foundation (awards CHE-1764409 and CHE-

2102425) for dielectric, light scattering and simulations work, and award DMR-1810194 for NMR

work. A.Kh. is thankful to the support by the Kazan Federal University Strategic Academic

Leadership Program

**Author contributions** 

H.Z., M.F. provided the sample. I.P., A.P.S. performed the dielectric measurements over a wide

range in frequency and analyzed the conductivity data. C.Z., L.M. performed the pulsed-field

gradient stimulated-echo sequence at high temperature. All authors contributed to the discussion

of the results.

**Corresponding Authors** 

§E-mail: sokolov@utk.edu, \*E-mail: ipopov@utk.edu

18

#### References

- [1] J. Popovic, Dry Polymer Electrolyte Concepts for Solid-State Batteries, Macromolecular Chemistry and Physics, 223 (2022) 2100344.
- [2] M. York, K. Larson, K.C. Harris, E. Carmona, P. Albertus, R. Sharma, M. Noked, E. Strauss, H. Ragones, D. Golodnitsky, Recent advances in solid-state beyond lithium batteries, Journal of Solid State Electrochemistry, 26 (2022) 1851-1869.
- [3] G. Deysher, P. Ridley, S.-Y. Ham, J.-M. Doux, Y.-T. Chen, E.A. Wu, D.H.S. Tan, A. Cronk, J. Jang, Y.S. Meng, Transport and mechanical aspects of all-solid-state lithium batteries, Materials Today Physics, 24 (2022) 100679.
- [4] H. Zhu, D.R. MacFarlane, J.M. Pringle, M. Forsyth, Organic Ionic Plastic Crystals as Solid-State Electrolytes, Trends in Chemistry, 1 (2019) 126-140.
- [5] D.R. MacFarlane, M. Forsyth, P.C. Howlett, M. Kar, S. Passerini, J.M. Pringle, H. Ohno, M. Watanabe, F. Yan, W. Zheng, S. Zhang, J. Zhang, Ionic liquids and their solid-state analogues as materials for energy generation and storage, Nature Reviews Materials, 1 (2016) 15005.
- [6] K.K. Sonigara, Z. Shao, J. Prasad, H.K. Machhi, G. Cui, S. Pang, S.S. Soni, Organic Ionic Plastic Crystals as Hole Transporting Layer for Stable and Efficient Perovskite Solar Cells, Advanced Functional Materials, 30 (2020) 2001460.
- [7] I. Popov, K. Biernacka, H. Zhu, F. Nti, L. Porcarelli, X. Wang, A. Khamzin, C. Gainaru, M. Forsyth, A.P. Sokolov, Strongly Correlated Ion Dynamics in Plastic Ionic Crystals and Polymerized Ionic Liquids, The Journal of Physical Chemistry C, 124 (2020) 17889-17896.
- [8] K. Biernacka, F. Makhlooghiazad, I. Popov, H. Zhu, J.-N. Chotard, C.M. Forsyth, R. Yunis, L.A. O'Dell, A.P. Sokolov, J.M. Pringle, M. Forsyth, Investigation of Unusual Conductivity Behavior and Ion Dynamics in Hexamethylguanidinium Bis(fluorosulfonyl)imide-Based Electrolytes for Sodium Batteries, The Journal of Physical Chemistry C, 125 (2021) 12518-12530. [9] K. Biernacka, F. Makhlooghiazad, I. Popov, H. Zhu, J.-N. Chotard, L.A. O'Dell, A.P. Sokolov, J.M. Pringle, M. Forsyth, Exploration of phase diagram, structural and dynamic behavior of
- J.M. Pringle, M. Forsyth, Exploration of phase diagram, structural and dynamic behavior of [HMG][FSI] mixtures with NaFSI across an extended composition range, Physical Chemistry Chemical Physics, 24 (2022) 16712-16723.
- [10] D.R. MacFarlane, J. Huang, M. Forsyth, Lithium-doped plastic crystal electrolytes exhibiting fast ion conduction for secondary batteries, Nature, 402 (1999) 792-794.
- [11] A. Abouimrane, P.S. Whitfield, S. Niketic, I.J. Davidson, Investigation of Li salt doped succinonitrile as potential solid electrolytes for lithium batteries, Journal of Power Sources, 174 (2007) 883-888.
- [12] K. Biernacka, D. Al-Masri, R. Yunis, H. Zhu, A.F. Hollenkamp, J.M. Pringle, Development of new solid-state electrolytes based on a hexamethylguanidinium plastic crystal and lithium salts, Electrochimica Acta, 357 (2020) 136863.
- [13] F. Chen, S.W. de Leeuw, M. Forsyth, Dynamic Heterogeneity and Ionic Conduction in an Organic Ionic Plastic Crystal and the Role of Vacancies, The Journal of Physical Chemistry Letters, 4 (2013) 4085-4089.
- [14] M. Forsyth, F. Chen, L.A. O'Dell, K. Romanenko, New insights into ordering and dynamics in organic ionic plastic crystal electrolytes, Solid State Ionics, 288 (2016) 160-166.
- [15] J. Huang, A. Hill, M. Forsyth, D. MacFarlane, A. Hollenkamp, Conduction in ionic organic plastic crystals: The role of defects, Solid State Ionics, 177 (2006) 2569-2573.
- [16] L. Jin, K.M. Nairn, C.M. Forsyth, A.J. Seeber, D.R. MacFarlane, P.C. Howlett, M. Forsyth, J.M. Pringle, Structure and Transport Properties of a Plastic Crystal Ion Conductor:

- Diethyl(methyl)(isobutyl)phosphonium Hexafluorophosphate, Journal of the American Chemical Society, 134 (2012) 9688-9697.
- [17] D.R. MacFarlane, M. Forsyth, Plastic Crystal Electrolyte Materials: New Perspectives on Solid State Ionics, Advanced Materials, 13 (2001) 957-966.
- [18] S.J. Pas, J. Huang, M. Forsyth, D.R. MacFarlane, A.J. Hill, Defect-assisted conductivity in organic ionic plastic crystals, The Journal of Chemical Physics, 122 (2005) 064704.
- [19] H. Zhu, M. Forsyth, Ion Vacancies and Transport in 1-Methylimidazolium Triflate Organic Ionic Plastic Crystal, The Journal of Physical Chemistry Letters, 11 (2020) 510-515.
- [20] H. Zhu, U.a. Rana, V. Ranganathan, L. Jin, L.A. O'Dell, D.R. MacFarlane, M. Forsyth, Proton transport behaviour and molecular dynamics in the guanidinium triflate solid and its mixtures with triflic acid, Journal of Materials Chemistry A, 2 (2014) 681-691.
- [21] J.C. Dyre, P. Maass, B. Roling, D.L. Sidebottom, Fundamental questions relating to ion conduction in disordered solids, Reports on Progress in Physics, 72 (2009) 046501.
- [22] P. Maass, M. Meyer, A. Bunde, Nonstandard relaxation behavior in ionically conducting materials, Physical Review B, 51 (1995) 8164-8177.
- [23] B. Roling, C. Martiny, S. Brückner, Ion transport in glass: Influence of glassy structure on spatial extent of nonrandom ion hopping, Physical Review B, 63 (2001) 214203.
- [24] E. Bychkov, Superionic and ion-conducting chalcogenide glasses: Transport regimes and structural features, Solid State Ionics, 180 (2009) 510-516.
- [25] I. Yokota, On the Deviation from the Einstein Relation Observed for Diffusion of Ag+ Ions in  $\alpha$ -Ag2S and Others, Journal of the Physical Society of Japan, 21 (1966) 420-423.
- [26] P. Adeli, J.D. Bazak, K.H. Park, I. Kochetkov, A. Huq, G.R. Goward, L.F. Nazar, Boosting Solid-State Diffusivity and Conductivity in Lithium Superionic Argyrodites by Halide Substitution, Angewandte Chemie International Edition, 58 (2019) 8681-8686.
- [27] P. Bron, S. Johansson, K. Zick, J. Schmedt auf der Günne, S. Dehnen, B. Roling, Li10SnP2S12: An Affordable Lithium Superionic Conductor, Journal of the American Chemical Society, 135 (2013) 15694-15697.
- [28] F. Hussain, P. Li, Z. Li, Theoretical Insights into Li-Ion Transport in LiTa2PO8, The Journal of Physical Chemistry C, 123 (2019) 19282-19287.
- [29] A. Marcolongo, N. Marzari, Ionic correlations and failure of Nernst-Einstein relation in solid-state electrolytes, Physical Review Materials, 1 (2017) 025402.
- [30] N.M. Vargas-Barbosa, B. Roling, Cover Feature: Dynamic Ion Correlations in Solid and Liquid Electrolytes: How Do They Affect Charge and Mass Transport? (ChemElectroChem 2/2020), ChemElectroChem, 7 (2020) 363-363.
- [31] K.R. Harris, M. Kanakubo, Revised and Extended Values for Self-Diffusion Coefficients of 1-Alkyl-3-methylimidazolium Tetrafluoroborates and Hexafluorophosphates: Relations between the Transport Properties, The Journal of Physical Chemistry B, 120 (2016) 12937-12949.
- [32] H. Tokuda, K. Hayamizu, K. Ishii, M.A.B.H. Susan, M. Watanabe, Physicochemical Properties and Structures of Room Temperature Ionic Liquids. 2. Variation of Alkyl Chain Length in Imidazolium Cation, The Journal of Physical Chemistry B, 109 (2005) 6103-6110.
- [33] H. Tokuda, S. Tsuzuki, M.A.B.H. Susan, K. Hayamizu, M. Watanabe, How Ionic Are Room-Temperature Ionic Liquids? An Indicator of the Physicochemical Properties, The Journal of Physical Chemistry B, 110 (2006) 19593-19600.
- [34] H.A. Every, A.G. Bishop, D.R. MacFarlane, G. Orädd, M. Forsyth, Transport properties in a family of dialkylimidazolium ionic liquids, Physical Chemistry Chemical Physics, 6 (2004) 1758-1765.

- [35] C. Gainaru, E.W. Stacy, V. Bocharova, M. Gobet, A.P. Holt, T. Saito, S. Greenbaum, A.P. Sokolov, Mechanism of Conductivity Relaxation in Liquid and Polymeric Electrolytes: Direct Link between Conductivity and Diffusivity, The Journal of Physical Chemistry B, 120 (2016) 11074-11083.
- [36] J.R. Sangoro, A. Serghei, S. Naumov, P. Galvosas, J. Kärger, C. Wespe, F. Bordusa, F. Kremer, Charge transport and mass transport in imidazolium-based ionic liquids, Physical Review E, 77 (2008) 051202.
- [37] S. Seki, K. Hayamizu, S. Tsuzuki, K. Fujii, Y. Umebayashi, T. Mitsugi, T. Kobayashi, Y. Ohno, Y. Kobayashi, Y. Mita, H. Miyashiro, S.-i. Ishiguro, Relationships between center atom species (N, P) and ionic conductivity, viscosity, density, self-diffusion coefficient of quaternary cation room-temperature ionic liquids, Physical Chemistry Chemical Physics, 11 (2009) 3509-3514.
- [38] N.A. Stolwijk, S. Obeidi, Combined analysis of self-diffusion, conductivity, and viscosity data on room temperature ionic liquids, Electrochimica Acta, 54 (2009) 1645-1653.
- [39] V. Bocharova, A.P. Sokolov, Perspectives for Polymer Electrolytes: A View from Fundamentals of Ionic Conductivity, Macromolecules, 53 (2020) 4141-4157.
- [40] A. Kisliuk, V. Bocharova, I. Popov, C. Gainaru, A.P. Sokolov, Fundamental parameters governing ion conductivity in polymer electrolytes, Electrochimica Acta, 299 (2019) 191-196.
- [41] S. Obeidi, N.A. Stolwijk, S.J. Pas, Mass and Charge Transport in a Cross-Linked Polyether-Based Electrolyte. The Role of Ion Pairs, Macromolecules, 38 (2005) 10750-10756.
- [42] E.W. Stacy, C.P. Gainaru, M. Gobet, Z. Wojnarowska, V. Bocharova, S.G. Greenbaum, A.P. Sokolov, Fundamental Limitations of Ionic Conductivity in Polymerized Ionic Liquids, Macromolecules, 51 (2018) 8637-8645.
- [43] F. Wieland, V. Bocharova, P. Münzner, W. Hiller, R. Sakrowski, C. Sternemann, R. Böhmer, A.P. Sokolov, C. Gainaru, Structure and dynamics of short-chain polymerized ionic liquids, The Journal of Chemical Physics, 151 (2019) 034903.
- [44] J.E. Bostwick, C.J. Zanelotti, C. Iacob, A.G. Korovich, L.A. Madsen, R.H. Colby, Ion Transport and Mechanical Properties of Non-Crystallizable Molecular Ionic Composite Electrolytes, Macromolecules, 53 (2020) 1405-1414.
- [45] C.Y. Son, Z.-G. Wang, Ion transport in small-molecule and polymer electrolytes, The Journal of Chemical Physics, 153 (2020) 100903.
- [46] B.K. Wheatle, N.A. Lynd, V. Ganesan, Effect of Polymer Polarity on Ion Transport: A Competition between Ion Aggregation and Polymer Segmental Dynamics, ACS Macro Letters, 7 (2018) 1149-1154.
- [47] Z. Zhang, B.K. Wheatle, J. Krajniak, J.R. Keith, V. Ganesan, Ion Mobilities, Transference Numbers, and Inverse Haven Ratios of Polymeric Ionic Liquids, ACS Macro Letters, 9 (2020) 84-89.
- [48] P.B. Ishai, M.S. Talary, A. Caduff, E. Levy, Y. Feldman, Electrode polarization in dielectric measurements: a review, Measurement Science and Technology, 24 (2013) 102001.
- [49] H.K. Kashyap, H.V.R. Annapureddy, F.O. Raineri, C.J. Margulis, How Is Charge Transport Different in Ionic Liquids and Electrolyte Solutions?, The Journal of Physical Chemistry B, 115 (2011) 13212-13221.
- [50] I. Popov, A. Khamzin, R. Matsumoto, W. Zhao, X. Lin, P.T. Cummings, A.P. Sokolov, Controlling ion transport number in Solvent-in-Salt Solutions, The Journal of Physical Chemistry B, (just accepted) (2022).

- [51] C.A. Angell, Diffusion—Conductance Relations and Free Volume in Molten Salts, The Journal of Physical Chemistry, 69 (1965) 399-403.
- [52] M. Braun, K.W. Kehr, Diffusivity and mobility of lattice gases in lattices with randomly blocked sites, Philosophical Magazine A, 61 (1990) 855-871.
- [53] J.O. Isard, The Haven ratio in glasses, Journal of Non-Crystalline Solids, 246 (1999) 16-26.
- [54] D.R. MacFarlane, M. Forsyth, E.I. Izgorodina, A.P. Abbott, G. Annat, K. Fraser, On the concept of ionicity in ionic liquids, Physical Chemistry Chemical Physics, 11 (2009) 4962-4967.
- [55] G.E. Murch, The haven ratio in fast ionic conductors, Solid State Ionics, 7 (1982) 177-198.
- [56] G.E. Murch, J.C. Dyre, Correlation effects in ionic conductivity, Critical Reviews in Solid State and Materials Sciences, 15 (1989) 345-365.
- [57] A. Noda, K. Hayamizu, M. Watanabe, Pulsed-Gradient Spin-Echo 1H and 19F NMR Ionic Diffusion Coefficient, Viscosity, and Ionic Conductivity of Non-Chloroaluminate Room-Temperature Ionic Liquids, The Journal of Physical Chemistry B, 105 (2001) 4603-4610.
- [58] R. Terai, R. Hayami, Ionic diffusion in glasses, Journal of Non-Crystalline Solids, 18 (1975) 217-264.
- [59] F. Chen, L. Jin, S.W. de Leeuw, J.M. Pringle, M. Forsyth, Atomistic simulation of structure and dynamics of the plastic crystal diethyl(methyl)(isobutyl)phosphonium hexafluorophosphate, The Journal of Chemical Physics, 138 (2013) 244503.
- [60] J.C. Dyre, The random free-energy barrier model for ac conduction in disordered solids, Journal of Applied Physics, 64 (1988) 2456-2468.
- [61] J.C. Dyre, Studies of ac hopping conduction at low temperatures, Physical Review B, 49 (1994) 11709-11720.
- [62] J.C. Dyre, T.B. Schrøder, Universality of ac conduction in disordered solids, Reviews of Modern Physics, 72 (2000) 873-892.
- [63] T.B. Schrøder, J.C. Dyre, Scaling and Universality of ac Conduction in Disordered Solids, Physical Review Letters, 84 (2000) 310-313.
- [64] T.B. Schrøder, J.C. Dyre, ac Hopping Conduction at Extreme Disorder Takes Place on the Percolating Cluster, Physical Review Letters, 101 (2008) 025901.
- [65] J.R. Sangoro, F. Kremer, Charge Transport and Glassy Dynamics in Ionic Liquids, Accounts of Chemical Research, 45 (2012) 525-532.
- [66] P.J. Griffin, A.L. Agapov, A.P. Sokolov, Translation-rotation decoupling and nonexponentiality in room temperature ionic liquids, Physical Review E, 86 (2012) 021508.
- [67] H.J. Schoenert, Evaluation of velocity correlation coefficients from experimental transport data in electrolytic systems, The Journal of Physical Chemistry, 88 (1984) 3359-3363.
- [68] K.R. Harris, Relations between the Fractional Stokes–Einstein and Nernst–Einstein Equations and Velocity Correlation Coefficients in Ionic Liquids and Molten Salts, The Journal of Physical Chemistry B, 114 (2010) 9572-9577.